Fusion Engineering and Design 197 (2023) 114069

Contents lists available at ScienceDirect

Fusion Engineering and Design

journal homepage: www.elsevier.com/locate/fusengdes

On the use of error field correction coils in JET

L. Piron [a,b,*], M. Baruzzo [c], L Baylor [d], C D Challis [e], M.P. Gryaznevich [e,1], T.C. Hender [e], R.B. Henriques [f], N. Hawkes [e], S. Jachmich [g], E. Joffrin [h], M. Lehnen [g], M. Lennholm [e], Y.Q. Liu [i], J. Mailloux [e], L. Moreira [e,1], D. Valcarcel [e], JET Contributors[2]

[a] Dipartimento di Fisica "G. Galilei", Università degli Studi di Padova, Padova, Italy
[b] Consorzio RFX, Corso Stati Uniti 4, 35127, Padova, Italy
[c] ENEA, Fusion and Nuclear Safety Department, C.R. Frascati, Rome, Italy
[d] Oak Ridge National Laboratory, Oak Ridge, TN 37831-6169, TN, USA
[e] United Kingdom Atomic Energy Authority, Culham Science Centre, Abingdon, Oxon OX14 3DB, UK
[f] Instituto de Plasmas e Fusão Nuclear, Instituto Superior Técnico, Universidade de Lisboa, Lisboa 1049-001, Portugal
[g] ITER Organization, Route de Vinon, CS 90 046, Saint Paul Lez Durance 13067, France
[h] Atomic Energy Commission, CEA, IRFM, Saint Paul Lez Durance F-13108, France
[i] General Atomics, P.O. Box 85608, San Diego, California 92186-5608, USA

ARTICLE INFO

Keywords:
JET
Control
Error field correction coil system

ABSTRACT

This work describes the usage of Error Field Correction Coil (EFCC) system [*Barlow I.* et al. *2001 Fusion Eng. Des. 58–59 189*], which is a set of 4 coils located external to the vessel of the JET device, with the aim of introducing non-axisymmetric $n = 1$ magnetic field perturbations in various targeted plasma experiments. Besides being used to characterize and correct the intrinsic error field, the EFCCs system has been exploited to i) probe plasma stability in high-β_N regimes through the MHD spectroscopy technique, allowing the identification of resistive-wall mode stable operational scenarios, ii) study radiation asymmetry when testing the shattered pellet injector as the prime candidate for ITER disruption mitigation system, and iii) control edge localized modes, permitting a reduction in heat fluxes and carbon erosion of the divertor target plates.

1. Introduction

Magnetic fusion devices are often equipped with non-axisymmetric coils, located internal and/or external with respect to the vessel, to induce magnetic field perturbations. Depending on the number of mounted coils, located possibly in two or three toroidal rows, and of power supplies available, magnetic fields perturbations with various m/n spectra (m/n is the ratio between the poloidal/toroidal mode numbers) can be induced, altering the plasma behavior in various ways.

On one hand, magnetic field perturbations can, for example, be used to i) mitigate/suppress edge localized modes (ELMs) [1–5], while avoiding the degradation of the fast-ion confinement [6], ii) guarantee stable detachment operations [7], iii) probe plasma stability [8–18], iv) control and to force rotation of MHD modes [19,20], v) compensate spurious magnetic fields, i.e. error fields (EF) [21–25], vi) control runaway electrons [26] and vii) modify the onset of density limit disruptions [27].

On the other hand, externally applied magnetic field perturbations can affect negatively the plasma through various mechanisms, i.e. damping the toroidal flow, degrading particle confinement trough density pump-out, inducing excessive magnetic stochastization, increasing the threshold for L-H transition, destabilizing MHD modes and even inducing plasma disruptions [28].

To minimize such negative effects, when designing plasma experiments which foresee externally imposed 3-D fields, the coil current amplitude, spectra content, coil phasing among the coil rows, are fine-tuned, empirically and/or by the use of an electro-magnetic code coupled with plasma response modeling [29].

In this work, we present an overview of the use of the JET Error Field Correction Coils (EFCCs) [30], which is a set of 4 non-axisymmetric coils located outside the vacuum vessel [31]. Over the years, this system has been exploited for various purposes, such as probing MHD plasma

* Corresponding author.
E-mail address: lidia.piron@unipd.it (L. Piron).
[1] Present affiliation Tokamak Energy Ltd., 173 Brook Drive, Milton Park, Abingdon OX14 4SD, UK.
[2] See the author list of "J. Mailloux et al., Nucl. Fusion 2022 for the JET Contributors".

https://doi.org/10.1016/j.fusengdes.2023.114069
Received 2 July 2023; Received in revised form 23 October 2023; Accepted 13 November 2023
Available online 18 November 2023

stability, studying radiation asymmetry when testing the shattered pellet injector (SPI), the disruption mitigation system (DMS) for ITER, identifying and correcting the intrinsic EF and performing ELM control studies. In particular, the manuscript is structured as follows: Section 2 presents the EFCCs system in detail; Section 3 summarizes the series of experiments aforementioned, which exploited the EFCCs system and finally, Section 4 gives the conclusions.

2. The error field correction coil system

On JET, external non-axisymmetric magnetic fields can be applied by the Error Field Correction Coil system (EFCCs), made up of four coils, spanning each 70 deg in toroidal angle and with a radial distance along the winding of 5.3 to 7 m from the axis of the machine, arranged symmetrically around the vacuum vessel and external to it. A perspective view of EFCCs system is shown in Fig. 1(a). The coils are located in octants 1, 3, 5 and 7 of the vessel; each coil has 16 turns and it carries a maximum of 6 kA in a single turn.

The EFCCs can be wired in $n = 1$ and $n = 2$ configurations. The $n = 1$ configuration, used in some experiments presented in this work, is induced by feeding EFCCs with oppositely directed currents in toroidally opposite coils. The induced magnetic field perturbations can have various fixed toroidal phases, by varying the EFCC current polarities in the quadrature pairs of coils.

Originally, the EFCCs system was designed for compensating the intrinsic error field arising from asymmetries in the poloidal field coils due to the presence of feedthroughs [30,32], replacing the internal saddle coils which were disabled during the 2004 JET shutdown because they suffered many hardware failures, most severely with frequent in-vessel earth leaks [33].

Studies on error fields on JET show that the amplitude of the intrinsic error field is relatively small: the locked mode threshold in 1.9 MA plasma current, 2 T toroidal field plasmas is approximately $B_{2,1}/B_T \approx 9.6\ 10^{-5}$, where $B_{2,1}$ is the 2/1 radial magnetic field component and B_T is the toroidal field [34–38]. For EF correction, EFCC current of approximately 130 A was envisaged in one coil pair, the 3,7 EFCC, and −60 A EFCC current in the other one, the 1,5 EFCC [38].

A characterization of the frequency response of the JET wall to externally applied $n = 1$ magnetic field perturbations in vacuum has been carried out, by performing dedicated vacuum discharges and by calculating the $n = 1$ radial magnetic field (B_r) amplitude and phase, obtained linearly combining normal magnetic field signals from a subset of four saddle loops located in identical poloidal locations, 90 ° apart in the toroidal direction, mounted on the low field side midplane of the vacuum vessel and placed below the EFCC coils. A sketch of EFCCs and saddle loop sensors in JET device is shown in Fig. 1(b).

The frequency response of the JET wall has been identified analyzing a database of both carbon (C) and ITER-like Wall (ILW) vacuum discharges to assess if the change of JET wall, which took place in 2008 [39], affects the magnetic field penetration, and so the eddy currents pattern induced in the vessel wall.

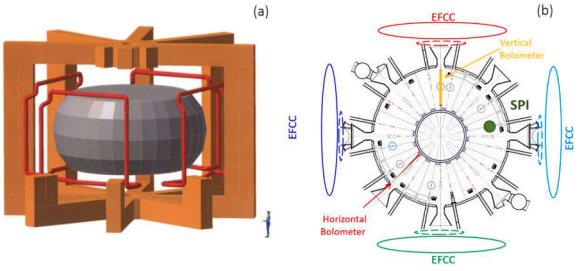

Fig. 1. (a) Perspective view of JET showing the error field correction coils (in red). (b) Toroidal view of the error field correction coils (solid colored lines) and the corresponding saddle loop sensors (dashed lines), together with the location of bolometry diagnostics and the shattered pellet injector (SPI).

An example of a JET-C experiment in vacuum is reported in Fig. 2(a, b), where the time behavior of EFCC current rotating at 30 Hz is shown in the top panel and the induced $n = 1$ magnetic field, in the bottom one, as measured by a combination of midplane saddle loop signals located in the same octants as the EFCCs. Several vacuum shots with magnetic field perturbations rotating at frequencies up to 100 Hz have been analyzed. In this way, the transfer function between EFCCs and midplane saddle loops can be calculated.

The transfer function experimentally identified is reported in Fig. 2 (c,d), where the blue symbols correspond to C wall data, the red ones to ILW. The data from vacuum C wall discharges matches well those of ILW, therefore it is possible to conclude that the penetration of the external magnetic field is not sensitive to the change of wall material in JET.

The MARS-F code [40] has been benchmarked against these data. To retrieve a good match between the experimental results and MARS-F modeling, a model with two shells has been implemented in the code. In particular, the first shell, which corresponds to the JET vacuum vessel, has been located at $r = 1.3$ a, where a is the minor radius of JET and equals to 0.459 m. On the other hand, the second shell is at $r = 1.7$ a, and approximately corresponds to the location of the JET mechanical support structure. In this case, the shell has a thin structure, with a poloidal gap covering about 10 % of the total poloidal circumference, and with the wall time 10 times larger than the JET wall time. The resistivity in this gap has been increased by a factor 100 with respect to the other region. The fit achieved with this double shell model is reported in Fig. 2(c,d) with a dashed green line and is in good agreement with experimental trends.

3. Experiments with error field correction coils

In this section, we provide an overview of experiments where the presence of EFCCs has been exploited for targeting various physics studies.

a) *EFCCs used to probe plasma stability*

Stability at high plasma pressure is an important requisite for advanced tokamak plasma scenarios, such as those foreseen for ITER and compatible with the steady-state operation of future reactors. Such scenarios rely on increased normalized beta (β_N) plasmas for efficient operation. Here β_N is defined as $\beta\ B_t\ a/I_p$, where β is the ratio of the plasma pressure to the magnetic field pressure, B_t the toroidal magnetic

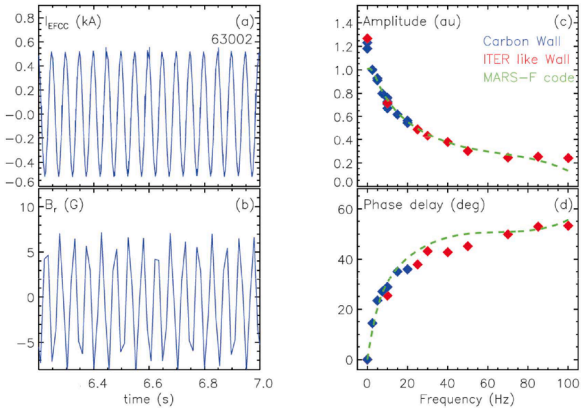

Fig. 2. Time behavior of (a) EFCC current and (b) $n = 1$ magnetic field as measured by a combination of signals of midplane saddle loops located in the same octants as the EFCCs. (c-d) Transfer function between the EFCCs and $n = 1$ connected saddle coils identified using JET-C wall (blue dots) and ILW data (red dots). The dashed green line corresponds to MARS-F code modeling.

field in T, a the minor radius in m and I_p the plasma current in MA.

As reported in [19], the resistive wall mode (RWM), which is a global kink-like, non-axisymmetric instability, has often been considered as a major obstacle to steady state operation in the advanced tokamak scenario. Although the presence of a conducting vessel wall tends to increase the β-limit, especially in low torque regimes, it is critical to ensure that the RWM stays stable when the plasma pressure exceeds the ideal no-wall beta limit, $\beta_N^{\text{no-wall}}$, the ideal β limit calculated in the complete absence of a wall [40–42].

A safe way of probing no-wall stability consists of examining the plasma response to externally applied magnetic fields though the so-called MHD spectroscopy technique. When the plasma pressure exceeds the no-wall β-limit, an enhancement of the Resonant Field Amplification (RFA) metrics, defined as the ratio of the plasma response to the externally applied magnetic field, occurs.

Looking for the RFA enhancement as an indicator of the no-wall limit has been used in scenario development of high−β experiments in several devices, such as DIII-D [8–10], C-wall JET [11–15], ASDEX Upgrade [16] and MAST [17] tokamaks and in RFX-mod reversed-field pinch [18].

Here, we report the use of the RFA technique to probe plasma stability in advanced tokamak scenarios in JET ILW plasmas. The discharge reported in Fig. 3 represents an experiment and refers to an $I_p = 1.55$ MA, $B_t = 2.4$ T plasma. As shown in Fig. 3(d), the $n = 1$ magnetic field perturbation has been induced by feeding the EFCCs with 200 A current oscillating at 30 Hz, the optimal frequency for probing plasma stability

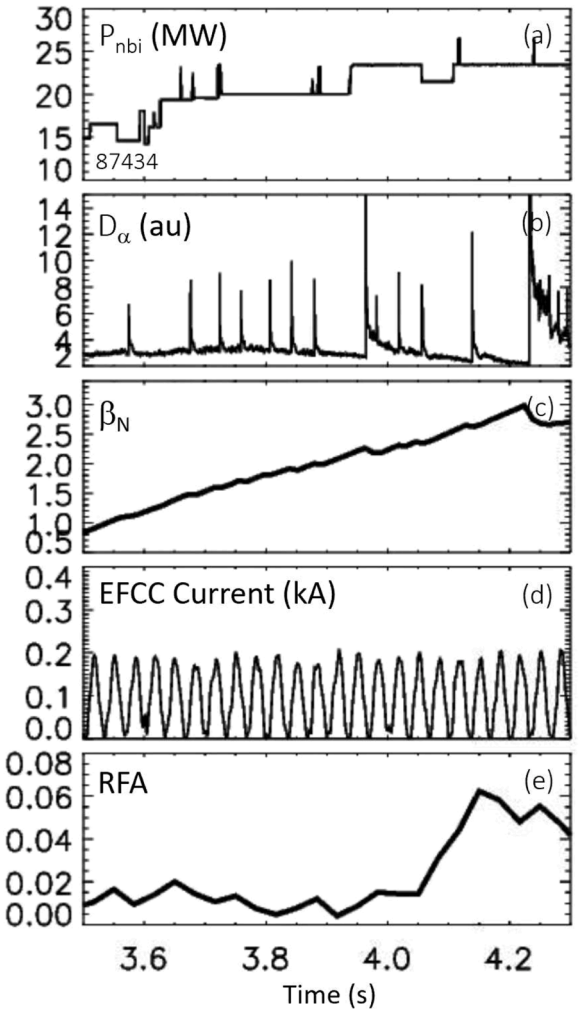

Fig. 3. Time behavior of (a) NBI power, (b) D_α, (c) β_N, (d) current in EFCCs and (e) RFA measurement of 87,434 JET-ILW plasma.

[14]. The induced magnetic field perturbation was typically 5 times below the locked mode onset error field threshold and was not seen by any other diagnostics except magnetics.

The RFA metric has been calculated as the ratio of the total $n = 1$ radial magnetic field measured at a 90 deg-shifted toroidal angle with respect to the EFCC field, to the total $n = 1$ radial magnetic field measured with a toroidal phase alignment with the EFCC current. For the EFCC and sensor coil geometry in JET, the numerator represents the pure plasma response, while the denominator predominantly measures the vacuum field from the EFCC current.

The behavior of RFA as a function of time is reported in Fig. 3(e). The response of the plasma is significantly enhanced when β_N is around 2.3. The observed sharp increase of the RFA metrics, by a factor 3, indicates that the plasma is near the no wall beta limit.

After the increase of RFA and in concomitance of a giant ELM, around $t = 44.2$ s, a β collapse event happens, as shown in Fig. 3(c). Magnetic crashes associated with collapses are very fast events, with durations of the order of 0.5 ms, and in this case the sudden loss of diamagnetic stored energy is about 10 %.

A statistical analysis, reported in [43], highlights that beta collapse events happen when $\beta_N > 2.5$, the value for which the plasma pressure is beyond the no-wall beta limit as suggested by the RFA metrics. A detailed characterization of beta collapse events and their effects on plasma performances in ILW plasmas will be presented in a dedicated paper.

The plasma stability limit identified in advanced scenarios on JET-ILW plasmas has been compared with the results obtained during C wall operations when RFA measurements are available. As opposed to C wall plasmas, the RFA technique has been applied in a restricted database of discharges, characterized by q_{min} value around 1.7. In any case, it is possible to compare C wall and ILW results, since RFA measurements in C wall plasmas with $q_{min} \approx 1.7$ are available.

The dependence of the β_N, when the RFA increases sharply, on the minimum q is shown in Fig. 4. The value of q_{min} has been determined from the EFIT code [44] reconstruction which includes motional Stark effect and low-n MHD activity measurements as constraints.

In the figure, blue indicates C wall discharges, red ILW ones. The decrease of β_N with increasing q_{min} has been already reported in [14], and it is mainly due to the dependence of plasma stability on the current profile.

The new RFA data, collected during ILW experiments, follows the

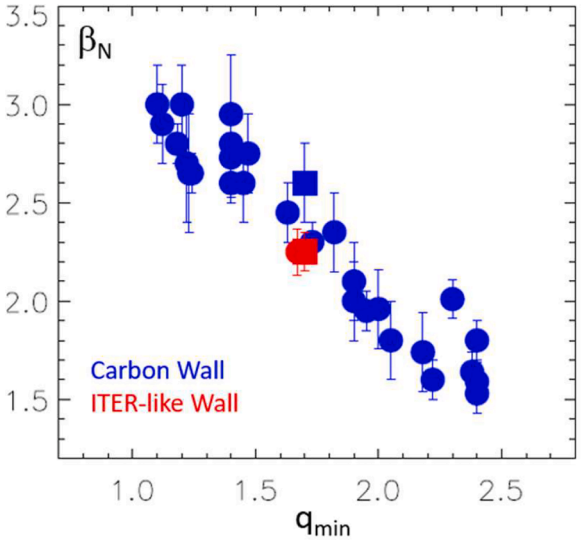

Fig. 4. β_N at the time instant when RFA shows a pronounced increase as a function of q_{min}. Each symbol type represents a different pulse. Blue dots correspond to C-wall plasmas, red ones to ILW ones.

same trend of the C wall ones. However, more data needs to be collected scanning various q values to confirm the same carbon wall dependence. Note that, the ILW RFA data is towards the lower end of the C data. Small changes in pressure and current density profiles between C and ILW cases, in particular close to the pedestal region, can indeed be responsible for changes in the RWM-driven beta limit [15].

a) *EFCCs used to study radiation asymmetry during mitigated plasma disruptions*

In order to reduce disruptions related risks in ITER, a DMS has been designed [45]. Such a system relies on the injection of a mixture of frozen material and gas, originating from the shattering of a cryogenic pellet on the surface of a bent pellet guide tube, the so-called SPI [46,47].

The SPI has the advantage with respect to the massive gas injection (MGI) of allowing for deeper and faster penetration of radiating material, as demonstrated on DIII-D [48] and on JET [47].

When a disruptive or pre-disruptive plasma state is detected, the SPI is triggered, resulting in a collimated spray of pellet material delivered to the torus. This spray of pellet material can dissipate a large fraction of the plasma thermal and magnetic energy through radiation, thus minimizing thermal loads on the tokamak first wall and divertor during the thermal quench, and mechanical stresses on the plasma facing components during the current quench [45,46,49]. Moreover, if the density rise due injected material is large enough, the collisional drag on seed runaway electrons is enhanced, allowing the suppression of large runaway beams [50,51].

In ITER one of the main concerns on disruption mitigation is the concentrated radiative load on the tokamak first wall and diagnostic equipment due to toroidal radiative asymmetries, which can affect the life-time of these components [46,47,49]. Experiments using both MGI and SPI, performed in various devices, as in Alcator C-mod [52], DIII-D [51], also supported by NIMROD modeling calculations [53,54], and JET [46,47] have shown that the radiation peaking distribution during the disruption process depends in particular on the relative phase of the gas/pellet shards injection with respect to the $n = 1$ O-point phase, which is the toroidal position of the of the center of the magnetic island.

In order to test the efficiency of the SPI concept in removing energy from the plasma fast enough and uniformly enough to effectively mitigate disruptions in ITER, an SPI system has been developed and tested at JET [47]. The system has the flexibility of delivering pellets in hydrogen, deuterium, neon and mixtures thereof with argon, at various velocities and with different shard size.

Among the SPI-related studies in support to ITER operation, a characterization of the toroidal distribution of the radiated power during induced disruptions in JET has been carried out. To perform this study, either a good toroidal coverage with the bolometry diagnostic is required, or the toroidal dependence of radiation can be deduced varying the location of the $n = 1$ O-point phase with respect to the injection location.

Because of the limited bolometry coverage at JET, the EFCCs system has been exploited to induce $n = 1$ 3D magnetic fields, at which the $n = 1$ mode is locked to. By varying the EFCC current polarities, the phase of the locked mode has been varied on a pulse-to-pulse basis. The SPI system has been triggered at a fixed time instant, as in H mode plasmas described in [47] or when the locked mode amplitude, or its time derivative, exceeded pre-set thresholds, as in the I_p=1.9 MA and B_t=2.1 T Ohmic discharges represented in Fig. 5.

In these discharges, during the plasma current flat-top the locked mode is induced by the application of $n = 1$ 3D fields with various phases by means of EFCCs while ramping down the plasma density, which favors the onset of the mode, as reported in figures (b, a), respectively.

In particular, the SPI system, which in this case injected 100 % neon pellets, was activated in real-time when the $n = 1$ amplitude of the locked mode was above 10.6 mT or its time derivative, calculated as a

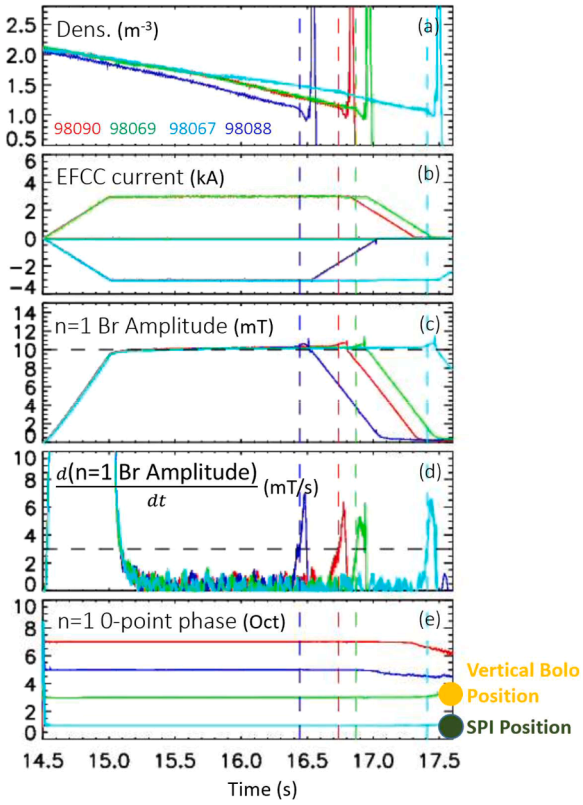

Fig. 5. Time behavior of (a) plasma density, (b) $n = 1$ EFCC current, (c) $n = 1$ Br amplitude, (d) time derivative of the $n = 1$ Br amplitude and (e) $n = 1$ O-point phase of a series of I_p=1.9 MA discharges with externally applied magnetic field perturbations with various toroidal phases.

first order transfer function, is above 3 mT/s, as shown in Fig. 5(c,d). The time of SPI triggering has been represented with a vertical dotted line in the figure.

It is interesting to note that a sudden increase of the normal magnetic field component, associated with the locked mode onset, is observed earlier in the discharge highlighted in blue in the figure. This is due to the fact that the toroidal phase of the external field coincides with the toroidal phase of JET intrinsic EF, as reported in [55] and discussed in the next subsection, and this amplifies the magnetic island triggering. Conversely, when the toroidal phase is opposite to the toroidal phase of the intrinsic error field, as in the plasma highlighted in cyan, the sudden increase of the normal magnetic field component occurs later on, being the intrinsic error field partially compensated by the external field.

After the SPI is fired, the pellet enters the plasma travelling at around 300 m/s, causing the plasma thermal quench, which occurs in time scales of the order of 1 ms, and the current quench, a fast current descent with typical duration of a few tens of milliseconds. During these events, the plasma energy was released as radiation, which has been detected by the vertical and horizontal bolometry diagnostics, whose toroidal position is represented in Fig. 1(b).

Fig. 6 represents the time behavior of the vertical and horizontal radiation of the discharges reported in Fig. 5, i.e. $P_{rad}^{vertical}$ and $P_{rad}^{horizontal}$, after the SPI triggering. Note that the radiation increase depends on the toroidal position of the locked mode with respect the location of the SPI and the bolometry diagnostics. For example, the discharge highlighted in cyan in Fig. 5 shows the fastest radiation increase, of about 5 ms after the SPI triggering, where the O-point phase of the locked mode is in front of the SPI, located in octant 1, and relatively close to the vertical bolometry fan, in octant 2.

By calculating the radiation asymmetry factor, defined as $P_{rad}^{vertical} - P_{rad}^{horizontal} / (P_{rad}^{vertical} + P_{rad}^{horizontal})$, and by using an

interpretative 1D radiation model, described in [46,47], which assumes a Gaussian-like impurity density and cosine-dependence for $n = 1$ mode, the toroidal peaking factor (TPF), i.e. e the maximum radiated power at a specific toroidal location over the averaged radiated power, can be deduced. The TPF is an important parameter, which needs to be quantified in existing devices equipped with an SPI system, to access the tolerable radiation peaking towards ITER operation to avoid damage of plasma facing components and diagnostic equipment. In particular, at JET dedicated studies are carrying out to identify a possible scaling of the TPF with the thermal plasma content, using pellet with various injected velocities, which will be documented in a separated publication.

a) *EFCCs used to correct JET intrinsic error field.*

The JET device is characterized by the presence of an intrinsic EF, associated with the feedlines in the poloidal field coils [32,35].

The impact of such a spurious magnetic field on hybrid and baseline plasma scenarios, the main operation regimes explored during the JET DT campaign, has been investigated statistically [55].

The analysis shows that a large fraction of disruptions in JET induced by the disruption mitigation valve (DMV), is associated with the presence of a tearing mode, which slows down due to wall image currents and then finally locks, increasing in amplitude. In particular, the DMV is activated when the locked mode amplitude normalized to the plasma current is above 0.2 mT / MA. When this threshold is reached, a trigger is passed to the disruption protection system high voltage power supply which induces a current into the DMV coil causing the valve to open and to inject the gas into the plasma. As a result, the radiation increases due to the interaction between the injected gas and the plasma, which effectively reduces the plasma energy, avoiding thus damage to vital plant components and structures.

The onset of the locked mode occurs in the plasma current ramp up phase in the early experiments aimed at performing hybrid scenarios presented here, and in the plasma ramp down in baseline plasmas. The dynamics of the locked mode is quite reproducible. As a matter of fact, no clear dependence of the $n = 1$ O-point phase and of $n = 1$ normalized mode amplitude on density and q_{95} has been observed, as shown in Figs. 7 (a,b) and (c,d), respectively. In the figure, the color code has been used to distinguish 2 ensembles of discharges analyzed: red represents 12 hybrid discharges, which exhibit a locked mode disruption during the plasma current ramp-up phase, green represents 70 baseline discharges, which exhibit a locked mode disruption during the plasma current ramp-down phase. Each point corresponds to the median of the distribution of the aforementioned quantities, while the bar corresponds to the 25th and the 75th percentiles of the distribution.

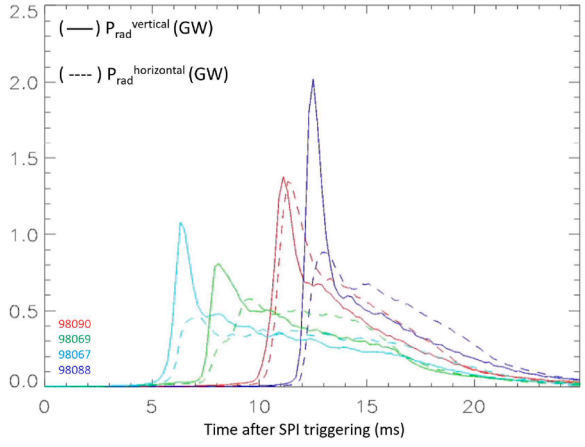

Fig. 6. Time behavior of radiation from vertical (solid line) and horizontal (dotted line) signals after SPI triggering. The database of discharges is the same as in Fig. 5.

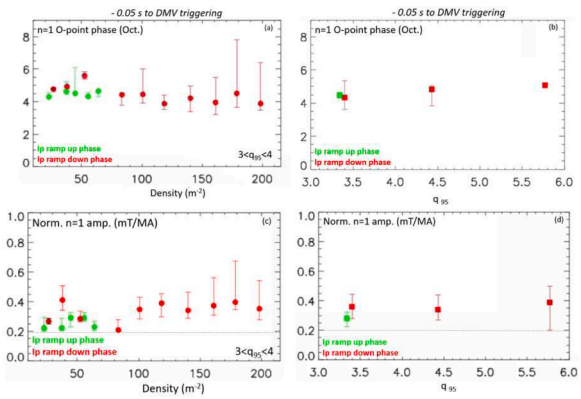

Fig. 7. $n = 1$ O-point phase and normalized $n = 1$ mode amplitude as a function of (a, c) density and (b, d) q_{95}, respectively, 0.05 s before the DMV triggering. The dotted line in panels (c-d) represents the threshold for DMV triggering.

The statistical analysis reveals that the $n = 1$ O-point phase is not equally distributed around the toroidal angle, but is localized around octants 4–5. This evidence is also confirmed by considering the normalized distribution function of the $n = 1$ O-point phase at various instants before the DMV triggering, reported in Fig. 8. In both the ensembles of discharges analyzed, the $n = 1$ O-point phase is localized around octants 4–5, indicating the presence of an intrinsic error field.

The presence of such an error field induces a braking of the mode rotation up to the mode locking. It is worth stressing that the mode locking could be avoided if the plasma rotates thanks to the field shielding mechanism [56]. However, neutral beam injection, which is the main source of plasma rotation in JET, can neither be applied during plasma current ramp up, nor in the plasma current ramp down phase, due to plasma scenario constraints.

To avoid disruptions, in this case, potentially two approaches can be pursued: the first one is avoiding the onset of the tearing mode, the second one is avoiding the mode locking mechanism to occur.

Regarding the first approach, an optimization of the plasma current ramp up has been adopted, which envisaged an increase of density at the X point formation [57], avoiding the development of magnetic shear reversal. To monitor the equilibrium profile evolution, a metric based on electron temperature hollowness has been developed. This quantity, defined as $(T_{core}\text{-}T_{edge})/T_{core}$, where T_{core} and T_{edge} are the volume averaged temperature in the core and at the edge from the electron cyclotron emission (ECE) diagnostic [58,59], triggers an alarm when is above an empirically defined threshold, thus allowing a safe plasma termination, if the plasma is moving toward conditions prone to tearing mode destabilization.

The second approach proposed aims at avoiding the locking mechanism itself, by correcting the intrinsic EF. Here, we report a set of experiments where the EFCC currents have been ramped up initially to induce a locked mode. Afterwards, the optimal correction currents for

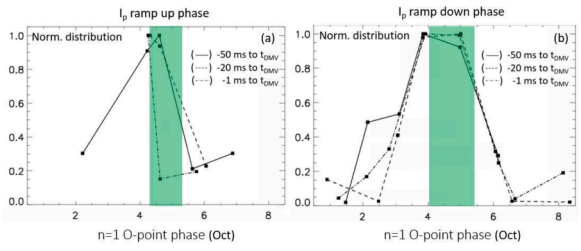

Fig. 8. Normalized distribution of the $n = 1$ O-point phase at various instants from the DMV triggering during plasma current ramp phase (a) and during plasma ramp down phase (b).

EF compensation has been successfully applied to prevent mode locking.

Fig. 9 compares two discharges with $I_p = 1.9$ MA, $B_t = 2$ T in which the EFCC system has been used to study plasma displacement in presence of 3D external magnetic fields [38]. Within this target, error field correction studies have been performed as well. EFCC currents have been used to induce a locked mode, by ramping up the current. The EFCC current should be larger than 0.8 kA to induce a locked mode in this plasma scenario. Indeed, the discharge highlighted in red in the figure does exhibit a locked mode as it can be detected by the change of slope of the $n = 1$ Br amplitude reported in Fig. 9(d). Conversely, the discharge highlighted in black, where lower EFCC currents have been applied, does not show a locked mode. After the mode locking was triggered, the optimal error field correction currents for the intrinsic error field have been applied and correspond to 130 A in the EFCC pair located in octants 3 and 7, and −60 A in the other EFCC pair, in octants 1 and 5 [38].

Eventually, the application of these EFCC currents is able to spin up the mode, which rotates at a few Hz. This experimental evidence proves that by controlling the EF, the mode locking mechanism can be avoided. This paves the way of using the EFCCs system to avoid locked mode disruptions. Forthcoming experiments are planned at JET to assess the reliability and the robustness of EF correction for DMV trigger avoidance.

a) *EFCCs used to edge localized mode control*

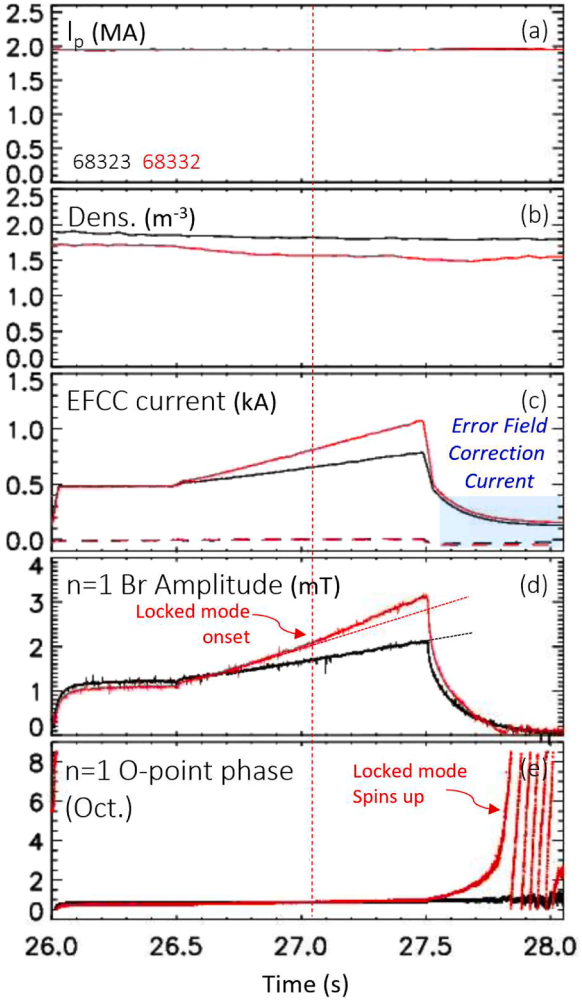

Fig. 9. Time behavior of (a) plasma current, (b) density, (c) EFCC coil currents, (d) $n = 1$ Br amplitude and (e) $n = 1$ O-point phase.

Edge localized modes (ELMs) are MHD periodic instabilities inherently present in high confinement plasmas and associated with the presence of large edge current densities and steep pressure gradients [1–5]. ELMs cause detrimental heat and particle fluxes onto plasma facing components, so posing a threat for the integrity and lifetime of these components [2]. On another hand, ELMs are useful to flush impurities out of the plasma and therefore controlling the frequency and amplitude of the ELMs is an advantage for plasma operation. A possible method to control ELMs consists in applying external magnetic field perturbations. Such a method allows for ELM mitigation or completed ELM suppression [60–64].

In JET Carbon wall, ELM control has been investigated by applying mainly $n = 1$ external magnetic field perturbations by means of EFCCs. As documented in [5], such a study has been carried out in plasmas with I_p up to 2.0 MA, high triangularity up to 0.45, β_N up to 3.0, and q_{95} in the range 3.0–- 4.8. With the application of $n = 1$ magnetic field perturbations, ELM mitigation has been achieved. The frequency of ELMs has been indeed increased by a factor of 4, allowing a reduction in heat fluxes on and carbon erosion of the divertor target plate.

ELM control by using externally applied $n = 2$ magnetic field perturbations has been attempted, as well, in plasmas with B_t =1.6 T, I_p = 1.6, 1.25 and 1.1 MA, so q_{95} varied between 3.1 and 4.5. Also in this case, ELM mitigation has been obtained and the frequency of ELMs has been increased by a factor of 3.5.

It is worth documenting that the triggering of the first ELM, which defines the transition from L to H mode, can be detected by analyzing the time behavior of the RFA indicator, defined in subsection a). Indeed, an increased RFA has been observed not only at high β_N in C and ILW plasmas, but at low β_N, as well.

This evidence is shown in Fig. 10, which reports the time behavior of β_N and D_α signals and the RFA metrics of a C wall plasma in panels (a-b) and of an ILW one, in (d-e). While the RFA metrics as a function of β_N is plotted in Figs. 10 (c-f).

Note that the first RFA peak occurs at β_N values about 2.1 and 1.2, for the C and ILW plasmas, respectively, considerably below the no-wall beta limit, which is about 2.8 and 2.3. This behavior is connected with the development of the edge current density during the ELM-free period, which destabilizes the $n = 1$ ideal peeling mode. This mode couples with the internal $n = 1$ mode lowering the stability limit, thus increasing the RFA [64].

By comparing Figs. 10 (a-c) with Figs. 10 (d-f), it is possible to notice that in ILW plasmas, the first ELM appears at lower β_N with respect to the C wall one. This is because during ILW operations increased deuterium gas rates are used compared to JET-C operation in order to avoid large

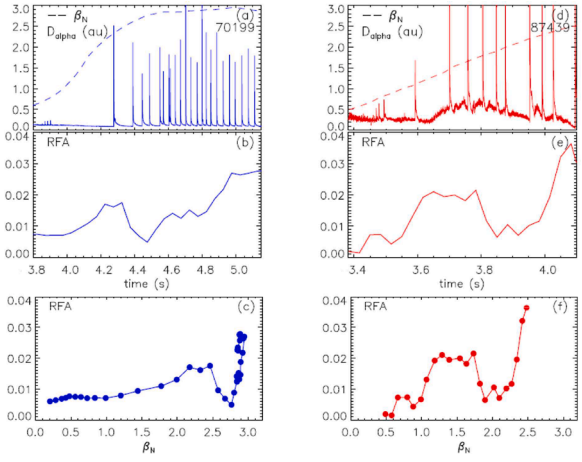

Fig. 10. Time behavior of (a-d) β_N and D_α,(b-e) RFA versus time and (c-f) RFA a function of β_N. The blue traces refer to a C wall plasma, instead the red ones to an ILW experiment.

impurity influxes of tungsten into the plasma [65,66].

4. Summary and conclusions

In this work, an overview on the use of the EFCC system in JET in various physics targeting plasma experiments has been reported.

In vacuum shots, a characterization of the frequency response of the wall to $n = 1$ magnetic field perturbations applied by means of EFCCs has been carried out, demonstrating that the change of the wall from carbon to a combination of beryllium and tungsten has no effects on the $n = 1$ magnetic field penetration. In the end, very small strips (poloidal limiters) spread around the torus have been added in the ITER-like wall, resulting in a not so large area comparing with the actual vessel and metallic structure supporting the TF coils.

In presence of plasma, the EFCCs system has been exploited to investigate plasma stability, both in carbon wall and ILW plasmas, through the RFA indicator, defined as the ratio of plasma response and the externally applied magnetic field. The RFA indicator increases not only when the plasma is approaching the β_N $^{\text{no-wall}}$, in high plasma pressure regimes, but also before the triggering of the first ELM, at low plasma pressure.

In JET, by using EFCCs to induce $n = 1$ and $n = 2$ magnetic fields, ELM mitigation has been achieved. The frequency of ELMs can indeed increase by up to a factor of 4 with a similar reduction in ELM energy loss [5].

EFCCs have also been tested to ameliorate the intrinsic error field by applying an opposing non-axisymmetric magnetic field. Error field correction allows for locked mode spinning up, paving the way to avoid locked mode disruptions.

Recently, the EFCCs system has been used to induce a locked modes located at various toroidal locations for radiation asymmetry studies related to MGI and SPI tests for ITER [47,51].

Despite the restricted coils coverage with respect to the one designed in ITER, which consists of 3 rows of 6 superconducting coils each, located external to the vessel [63,67], the JET error field correction system allows the achievement of interesting and important engineering and physics insights in preparation to ITER operation.

CrediT Author Statement

L. Piron: Writing- Reviewing and Editing, Conceptualization, Methodology, Formal analysis, Validation.

M. Baruzzo, L. Baylor, C. D. Challis, M.P. Gryaznevich, T.C. Hender, R. B. Henriques, N. Hawkes, S. Jachmich, E. Joffrin, M. Lehnen, M. Lennholm, Y.Q. Liu, J. Mailloux, L. Moreira, D. Valcarcel and JET Contributors: Conceptualization, Methodology, Formal analysis, Validation.

Declaration of Competing Interest

The authors declare that they have no known competing financial interests or personal relationships that could have appeared to influence the work reported in this paper.

Data availability

Data will be made available on request.

Acknowledgments

This work has been carried out within the framework of the EUROfusion Consortium, funded by the European Union via the Euratom Research and Training Programme (Grant Agreement No 101052200 — EUROfusion). Views and opinions expressed are however those of the author(s) only and do not necessarily reflect those of the European Union or the European Commission. Neither the European Union nor the European Commission can be held responsible for them.

References

[1] H. Zohm, et al., Plasma Phys. Control. Fusion 38 (1996) 105.
[2] A. Loarte, et al., Nat. Phys. 2 (2006) 369.
[3] H. Wilson, et al., Fus. Sci. Technol. 53 (2008) 161.
[4] P.B. Snyder, et al., Phys. Plasmas 9 (2002) 2037.
[5] Y. Liang, et al., Plasma Phys. Control. Fusion 49 (2007) B581.
[6] L. Sanchis, et al., Plasma Phys. Control. Fusion (2021). Accepted.
[7] M. Kobayashia, et al., Nuclear Mater. Energy 17 (2018) 137–141.
[8] A.M. Garofalo, et al., Phys. Plasmas 10 (2003) 4776.
[9] E.J. Strait, et al., Nucl. Fusion 43 (2003) 430.
[10] H. Reimerdes, et al., Phys. Rev. Lett. 93 (2004), 135002.
[11] T.C. Hender, et al., Resistive wall mode studies in JET, in: Proceeding 20th IAEA Fusion Energy Conf. 2004 (Vilamoura,Portugall, 2004), 2004 (Vienna: IAEA) IAEA-CN-116/EX/P2-22 CD-ROM file EX/P2-22.
[12] T.C. Hender, et al., Prediction of Rotational Stabilisation of Resistive Wall Modes in ITER, in: Proceeding. 21st IAEA Fusion Energy Conf. 2006 (Chengdu, China, 2006), 2006 (Vienna: IAEA) IAEACN-149/EX/P8-18 CD-ROM file EX/P8-18.
[13] H. Reimerdes, et al., Nucl. Fusion 45 (2005) 368.
[14] M.P. Gryaznevich, et al., Plasma Phys Control. Fusion 50 (2008), 124030.
[15] M.P. Gryaznevich, et al., Nucl. Fusion 52 (2012), 083018.
[16] V. Igochine, et al., Nucl. Fusion 57 (2017), 116027.
[17] I.T. Chapman, et al., Plasma Phys. Control. Fusion 53 (2011), 065022.
[18] D. Gregoratto, et al., Phys. Plasmas 7 (12) (2005), 092510.
[19] M.S. Chu M.S., M. Okabayashi, Plasma Phys. Control. Fusion 52 (2010), 123001.
[20] M. Okabayashi, et al., Nuclear Fusion 59 (2019), 126015.
[21] J.K. Park, et al., Phys. Rev. Lett. 99 (2007), 195003.
[22] J.L. Luxon, et al., Nucl. Fusion 43 (2003) 1813.
[23] J.E. Menard, et al., Nucl. Fusion 50 (2010), 045008.
[24] L. Piron, et al., Nucl. Fusion 63 (2011), 063012.
[25] L. Piron, et al., Fusion Eng. Des. 161 (2020), 111932.
[26] K.H. Finken, et al., Nucl. Fusion 47 (2007) 91.
[27] J.C. Vallet, et al., Phys. Rev. Lett. 67 (1991) 2662.
[28] J.D. Callen, Nucl. Fusion 51 (2011), 094026.
[29] L. Li, et al., Nucl. Fusion 56 (2016), 126007.
[30] F. Romanelli, et al., Nucl. Fusion 53 (2013), 104002.
[31] I. Barlow, et al., Fusion Eng. Des. 58-59 (2001) 189.
[32] G.M. Fishpool, et al., NF 34 (1994) 109.
[33] A. Santagiustina, H. Altmann, M. Buzio, D.J. Campbell, R. Claesen, G. D'Antona, et al., Operational experience with the JET saddle coil system, in: Proceeding of the 19th Symposium on Fusion Technology,Portugal Portugal, 1996.
[34] R.J. Buttery, et al., Nucl. Fusion 39 (1999) 1827.
[35] R.J. Buttery, et al., Nucl. Fusion 40 (4) (2000) 807.
[36] R.J. Buttery, et al., Phys Plasmas 19 (2012), 056111.
[37] D.F. Howell, et al., Bull. Am. Phys. Soc. 46 (2004) CP1.020.
[38] I.T. Chapman, et al., Nucl. Fusion 47 (2007) L36–L40.
[39] G.F. Matthews, et al., Phys. Scr. (2011), T14501400.
[40] Y.Q. Liu, et al., Phys. Plasmas 7 (2000) 3681.
[41] R. Fitzpatrick, Phys. Plasmas 9 (2002) 8.
[42] F. Troyon, et al., Plasma Phys. Control. Fusion 26 (1984) 209.
[43] E. Alessi, et al., MHD Analysis of Beta Collapses in AT JET Discharges, in: Proceeding 42nd EPS Conference on Plasma Physics, 22 - 26 July 2018, Lisbon, Portugal, 2015.
[44] L. Lao, et al., Nucl. Fusion 25 (1985) 1611.
[45] M. Lehnen, et al., in: R & D for reliable disruption mitigation in ITER 27th IAEA Fusion Energy Conference (FEC 2018), 2018 (Gandhinagar, India) EX/P7-12.
[46] M. Lehnen, et al., Nucl. Fusion 55 (2015), 123027.
[47] S. Jachmich, et al., Nucl. Fusion 62 (2022), 026012.
[48] N. Commaux, et al., Nucl.Fus 56 (2016), 046007.
[49] R.A. Pitts, et al., Journal Nuclear Material 463 (2015) 748.
[50] C. Reux, et al., Phys. Rev. Lett. 126 (2021), 175001.
[51] C. Paz-Soldan, et al., Plasma Phys. Control. Fusion 61 (2019), 054001.
[52] G.M. Olynyk, et al., Nucl. Fusion 53 (2013), 092001.
[53] D. Shiraki, et al., Nucl. Fusion 55 (2015), 073029.
[54] V.A. Izzo, et al., Nucl. Fusion 55 (2015) 07303.
[55] L. Piron et al., Experimental and modelling study of locked mode dynamics prior to disruptions in high performance JET plasmas, 46th EPS Conference on Plasma Physics, 8 -12 July 2019 Milan, Italy.
[56] R. Fitzpatrick, Phys. Plasmas 5 (1998) 3325.
[57] C.D. Challis, et al., Nucl. Fusion 60 (2020), 086008.
[58] M. Fontana, et al., Fusion Eng. Des. 161 (2020), 111934.
[59] L. Piron, et al., Fusion Eng. Des. 166 (2021), 112305.
[60] W. Suttrop, et al., Nucl. Fusion 58 (2018), 096031.
[61] T.E. Evans, et al., Nature Phys 2 (2006) 419.
[62] A. Kirk, et al., Nucl. Fusion 53 (2013), 043007.
[63] Y.M. Jeon, et al., Phys. Rev. Lett. 109 (2012), 035004.
[64] Y.Q. Liu, et al., Plasma Phys. Control. Fusion 51 (2009), 115005.
[65] M. Beurskens, et al., Nucl. Fusion 54 (2014), 043001.
[66] I. Nunes, et al., Plasma Phys Control. Fusion 58 (2016), 014034.
[67] Y. Gribov et al. Error Fields Expected in ITER and Their Correction ITR/P5-29.